# THERMAL RESPONSES OF TOKAMAK REACTOR FIRST WALLS DURING CYCLIC PLASMA BURNS

D. L. Smith and I. Charak
Argonne National Laboratory
Argonne, Illinois 60439

## Summary

The CINDA-3G computer code has been adapted to analyze the thermal responses and operating limitations of two fusion reactor first-wall concepts under normal cyclic operation. A component of an LMFBR computer code has been modified and adapted to analyze the ablative behavior of first-walls after a plasma disruption. The first-wall design concepts considered are a forced-circulation water-cooled stainless steel panel with and without a monolithic graphite liner. The thermal gradients in the metal wall and liner have been determined for several burn-cycle scenarios and the extent of surface ablation that results from a plasma disruption has been determined for stainless steel and graphite first surfaces.

## Introduction

In addition to extensive radiation damage and bulk heating from high-energy neutrons, the first wall of a tokamak fusion reactor will be subjected to high surface heat loads that may affect its integrity. For a tokamak reactor operating without a divertor, a heat flux equivalent to ∿ 25% of the neutron wall loading will be deposited in the surface regions of the first wall during a D-T plasma burn. Under normal operation, approximately 60% of this surface heat flux will be produced by particle transport from the plasma with the remaining 40% coming from electromagnetic radiation, primarily bremsstrahlung. The absorption and removal of these large surface heat fluxes pose a major problem in the design of a high-integrity first wall. In the event of a plasma disruption, essentially all of the thermal energy in the plasma and a fraction (depending on the electrical conductivity of the wall) of the stored magnetic energy in the plasma will be deposited in the surface regions of the first wall. Because of the inherent difficulties in repairing or replacing the first wall, it seems imperative that the first wall be designed to withstand a moderate number of disruptive events.

In the present investigation two models have been developed and existing computer codes have been adapted and used to evaluate the thermal responses and operating limitations of proposed first-wall concepts under normal (cyclic) and off-normal (plasma disruption) operation. The first-wall concepts considered include a forced-circulation-cooled stainless steel wall and a radiatively-cooled graphite liner. Appropriate materials property data used for the calculations have been obtained from the literature. The plasma performance and burn-cycle times considered are believed to be attainable in near-term experimental power reactors that operate without a divertor.[1,2] Thermally induced stresses in the first wall are a major concern during normal operation, whereas the extent of ablation of the first surface is the factor assessed for off-normal operation. The results obtained permit an evaluation of the relative merits of forced-circulation-cooled and radiatively cooled first walls.

Work supported by the Department of Energy.

## Model Development

Two models have been developed to analyze the thermal responses of proposed fusion reactor first-wall design concepts. One model considers the thermal responses of the first walls during cyclic plasma burns of ∿ 60 s. The second model considers the ablation of the wall material in the event of a plasma disruption. First wall concepts of the type proposed for near-term experimental power reactors that operate without a divertor have been analyzed.[1-3]

### First-Wall Geometry

Figure 1 is a schematic diagram of the forced-circulation-cooled metal first wall analyzed in the present investigation. This concept is a general case of the Argonne TEPR vacuum wall design.[2] It consists of a relatively thin (∿ 2 cm) metal slab with internal channels through which a coolant is circulated to remove the heat deposited in and on the wall. The first-wall may or may not also serve as the vacuum wall (the vacuum wall and coolant panel are of similar construction in the Argonne TEPR). In either case it is assumed that the metal wall provides some structural support and serves as a containment for the coolant. The coolant channels in this design are parallel to the front surface. Based on earlier results,[3,4] the coolant channels are located near the plasma-side surface and are closely spaced to minimize thermal gradients in the wall. The modular units of the metal wall are 0.8-cm wide with the coolant channels covering slightly less than 50% of the equivalent front surface. The irregular shape of the front face of the metal wall, which simulates the panel coil geometry proposed for the first wall, produces only a minor variation from a smooth wall.

A schematic diagram of the radiatively-cooled graphite liner is shown in Fig. 2. The liner is 1 cm thick and completely shields the structural wall from the plasma. The forced-circulation-cooled structural wall in this design is identical to the stainless steel wall described previously. Details of the liner support and the perturbations on the thermal gradients caused by the attachment of the liner to the structural wall have not been considered in the present investigation.

### Model for Cyclic Plasma Burn

The CINDA-3G computer code[5] has been adapted to calculate the thermal transients in the first wall during the cyclic plasma burn. CINDA-3G is a general-purpose three-dimensional code that solves the diffusion equation by finite-difference techniques. It is extremely flexible in that the user has available more than 100 built-in subroutines to accomplish a great variety of calculations. The present model incorporates (a) variable surface and bulk energy deposition in the wall, (b) the heat capacity of the wall material, (c) the heat conductance of the wall material, (d) thermal radiation for the case of the graphite liner, and (e) heat transport to the water coolant into the computer code to calculate the thermal response of the first wall.

Normal operation for the present analysis is a cyclic burn based on the calculated plasma performance for the Argonne TEPR.[1,6] The reference burn cycle consists of a 65-s pl[illegible] burn followed by a 15-s off-time for evacuati[illegible] the plasma chamber. Figure 3 shows a simplified [illegible]roximation of the power response that was deriv[illegible] from a complex power curve developed by Brooks.[6] The neutron power curve is represented by a ramp increase to a maximum wall loading of 1.6 MW/m$^2$ after 6 s, a ramp decrease to 0.75 MW/m$^2$ after 52 s, and a sharp ramp decrease to zero power at the end of the 65-s burn. This curve corresponds to an average neutron wall loading of 1 MW/m$^2$ for the duration of the burn. The total neutron power of ∿ 400 MW is indicated on the right-hand axis. The radiation and transport power is taken as 25% of the instantaneous neutron power.

The neutron energy is assumed to be deposited throughout the stainless steel wall giving a bulk heating rate that scales directly as the neutron wall loading. The bulk heating rate corresponding to a 1 MW/m$^2$ neutron wall loading is 10 W/cm$^3$ for stainless steel. The neutron flux, and hence the energy deposition, is attenuated exponentially through the stainless steel wall according to the results of Abdou.[7] The neutron heating in stainless steel is reduced to about 80% at the backside of the 2-cm wall. For the case of the graphite liner, a uniform bulk heating rate of 7 W/cm$^3$ is used for a 1 MW/m$^2$ neutron wall loading.[7] No attenuation of the neutron flux is assumed for the thin graphite liner.

In the present analysis it is assumed that all of the radiation and transport power is deposited on the surface of the first wall. This is considered to be a good approximation for the high-Z (atomic number) steel wall; however, the bremsstrahlung radiation from a high temperature plasma will have significant penetration (hundreds of micrometers) in low-Z materials such as graphite. Although this is not expected to be a major effect in the relatively thick monolithic graphite liner, it may have important implications for thin low-Z coatings such as beryllium.[2,4]

For the case of the forced-circulation-cooled metal wall the heat is simply transferred to the water coolant and transported out of the wall. For the case of the graphite liner, the energy deposited in the liner is thermally radiated to the metal structural wall and the heat again removed by the water coolant.

## Model for Plasma Disruption

An existing computer code, which was developed as a component of a larger Liquid Metal Fast Breeder Reactor (LMFBR) accident analysis code,[8] was appropriately modified and used to determine the extent of ablation of the first wall that will occur after a plasma disruption. This one-dimensional code treats the innermost, i.e., plasma side, region of the first wall as an ablative region. The thickness of this region is chosen such that some material remains under all conditions considered. The ablative region is subdivided into a desired number of subregions whereas the remainder of the wall is subdivided into two larger, equally-sized regions. Although one can account for heat loss from the wall, the time scale for the plasma dump is so short that, for practical purposes, a heat sink is ineffective. The majority of the energy deposited is accounted for by the heat capacity and the heat of vaporization (or sublimation) of the ablated subregions. Calculations have been made for both a stainless steel and a graphite first wall. Because the ablated regions are very thin (typically tens of micrometers) and the response time is very short (milliseconds), transport of any metal in the liquid form is not considered for the steel. The thin films are assumed to vaporize or resolidify in very short times. Sublimation of the graphite wall is assumed.

## Materials Property Data

The materials property data required for the calculation are summarized in Table I for stainless steel and graphite. Average handbook values are used for the densities. The thermal conductivity for stainless steel was taken from the temperature dependent equation for unirradiated material.[9] The thermal conductivity for graphite is sensitive to the type of graphite and to neutron radiation.[10-12] Data for irradiated graphite at elevated temperature (> 1000°C) range from 4 to 40 W/m·°K. A mean value of 10 W/m·°K has been used for the reference case. This value, which is representative of high grade graphite with 5-10% porosity, is used to account for effects expected from high helium generation. The specific heats given in the table are handbook values for the appropriate temperatures, viz., ∿ 500°C for stainless steel and ∿ 1000°C for graphite. The heats of vaporization (sublimation) are taken from thermodynamic tables and the emissivity of 0.8 is typical of many materials. Bulk neutron heating rates have been obtained from work of Abdou.[7,13]

## Thermal Response of First Wall

The thermal responses of the stainless steel wall and the graphite liner are determined for several burn-cycle scenarios and the extent of surface ablation that results from a plasma disruption is determined for stainless steel and graphite first surfaces.

### Response During Cyclic Plasma Burn

Energy deposition rates derived from Fig. 3 and the materials property data from Table I are incorporated into the CINDA-3G computer code to determine the thermal responses of the first walls for cyclic plasma burns. In the present investigation a plane that intersects the coolant channel has been analyzed. This plane is represented by the node points 38, 39, 41, 42, 57 and 60 in Figs. 1 and 2. Node 38 is on the plasma-side surface of the steel wall with nodes 39, 41, and 42 located in the steel wall at the positions indicated. Node 60 is on the plasma-side surface of the graphite liner and node 57 is on the back-side surface.

Figures 4-6 are plots of the thermal history for the four nodes in the steel wall during one burn cycle. Figure 4 represents the reference case with a 1 MW/m$^2$ neutron wall loading and an 80-s cycle time. Figure 5 shows the effect of increasing the off-cycle time from 15 s for the reference case to 30 s. Figure 6 is for the reference burn cycle but with a 2 MW/m$^2$ neutron wall loading. In all cases the coolant water temperature is ∿ 317°C. Table II summarizes some of the critical temperatures and ΔT's in the stainless steel wall. Although a stress analysis has not yet been conducted, a qualitative assessment of the thermal stress problem for the various burn-cycle scenarios can be obtained by comparing the variations in the temperature differences between nodes 38 and 39 and those between nodes 42 and 41. The longer off-cycle has very little effect on these temperature variations whereas the higher wall loading (2 MW/m$^2$) substantially increases the variations in the thermal gradients.

Figures 7-9 are plots of the thermal history for nodes 57 and 60 in the graphite liner during one burn cycle. The thermal response of the liner for the

reference burn cycle (1 MW/m$^2$, 80-s cycle) and mean thermal conductivity for graphite (10 W/m·K) is shown in Fig. 7. The effect of extending the off-time to 30 s (95-s cycle) is also shown in Fig. 7. Figure 8 shows the effect of variations in the thermal conductivity of graphite, and Fig. 9 shows the effect of increasing the wall loading to 2 MW/m$^2$. Critical temperatures and temperature differences obtained from this set of curves are summarized in Table III. The longer off-time slightly reduces the plasma-side surface temperature of liner and the ΔT through the liner. The thermal response of the liner is strongly dependent on the thermal conductivity of the graphite for the range of values considered. For the low conductivity (4 W/m·K), the maximum surface temperature approaches 1880°C, which is probably unacceptable because of excessive thermal vaporization, and the maximum ΔT through the wall is nearly 600°C. This low value of thermal conductivity may be reached for highly irradiated graphite with its inherently high helium generation rates. The results are substantially different when the high thermal conductivity is used. Calculations for the 2 MW/m$^2$ neutron wall loading also give high values for the maximum surface temperature (2123°C) and the ΔT through the wall (516°C). This result indicates that the maximum acceptable neutron wall loading for a radiatively cooled graphite liner is substantially less than 2 MW/m$^2$.

Figure 10 shows a comparison of the thermal responses for the surface regions of the forced-circulation-cooled stainless steel wall with and without the graphite liner. Both the maximum temperature of the steel surface and the maximum thermal gradient in the surface regions of the steel wall are significantly decreased by the liner. This indicates that the thermal fatigue problem associated with a stainless steel first wall[4] would be reduced if a radiatively cooled liner is used. However, the lifetime of the graphite liner relative to that of the steel wall has not been evaluated for the conditions indicated.

## Response after Plasma Disruption

The appropriate materials parameters have been incorporated into the plasma dump computer code to calculate the extent of ablation of the first wall in event of a plasma disruption. In the present calculation both the plasma thermal energy and the stored magnetic energy in the plasma, which are about equal, are deposited on the surface of the first wall during the dump. The time required for the plasma dump to occur and the wall area upon which the energy is deposited are not well known and probably vary with types of plasma instability. Therefore, the extent of ablation of the stainless steel and graphite walls has been calculated parametrically in terms of the dump time and the effective wall area over which the energy is deposited. Calculations have been carried out for an energy dump from a plasma that yields a 1 MW/m$^2$ neutron wall load. Thicknesses of the ablated regions as functions of the two parameters are shown in Figs. 11 and 12 for stainless steel and graphite, respectively. An instantaneous dump, i.e., zero dump time, does not allow for heat removal from the ablated region and, therefore, gives a maximum ablation thickness for a particular fractional wall area. For dump times up to 0.1 ms, the thicknesses of the ablated regions do not differ appreciably from the instantaneous dump curves. However, the 10 ms curve shows a substantial decrease in the amount of ablated material.

The fractional area of the first wall over which the plasma energy is deposited is critical. It is believed that the energy will be deposited over a major fraction (> 50%) of the wall area. For the reference case, i.e., 1.0 ms dump time, less than 50 μm of the steel wall will be ablated if the plasma energy is deposited over at least 50% of the wall. It is assumed that the deposition time is short enough and the depth of the affected region is so small that only vaporization of the steel is important. Significant transport of metal in the liquid phase is not considered for the thin regions and short dump times of interest. The ablation of graphite is generally less than half that of stainless steel for similar conditions of dump time and effective wall area. If the plasma energy is deposited over at least 50% of the wall, the maximum ablated region is less than 30 μm for graphite.

Since all of the stored magnetic energy will probably not be deposited on the surface of the first wall, the curves in Figs. 11 and 12 are conservative. Even so, results of these calculations indicate that first walls of stainless steel or graphite should withstand a moderate number of plasma disruptions if the plasma energy is effectively distributed over more than 25% of the reactor wall. This is true even if no credit is taken for redeposition of the ablated material, which is expected to occur. Also, an estimate of the capability of other first-wall materials to withstand plasma disruptions can be obtained by inserting relevant property data into the models.

## Conclusions

The CINDA-3G computer code[5] has been adapted to analyze the thermal responses and operating limitations of two fusion reactor first-wall concepts under normal cyclic plasma burns. The first-wall design concepts considered are a forced-circulation water-cooled stainless steel panel with and without a graphite liner. For a reference burn cycle with an average neutron wall loading of 1 MW/m$^2$ and a coolant temperature of 317°C, the maximum surface temperature in the steel wall was 402°C and the maximum ΔT in the first 0.175 cm of the wall was 48°C. These values increased to 479°C and 87°C, respectively, for a 2 MW/m$^2$ wall loading. For the reference case the maximum surface temperature of the graphite liner was 1545°C and the maximum ΔT through the 1-cm liner was 256°C. However, these values change substantially when the thermal conductivity of graphite is varied over the range of uncertainty, viz., 4-40 W/m·°K for irradiated graphite at > 1000°C. The surface temperature of the graphite becomes unacceptably high (> 2000°K) if the lower value of thermal conductivity is used or if the neutron wall loading is increased to 2 MW/m$^2$ with an average value of 10 W/m·°K for the conductivity of graphite.

A component of an LMFBR computer code[8] has been modified and adapted to analyze the ablative behavior of stainless steel and graphite first walls subjected to a plasma disruption. The thicknesses of ablated regions were determined parametrically for the two wall materials in terms of the plasma dump time and the fraction of the wall area over which the energy was deposited. If the plasma thermal energy and stored magnetic energy are deposited over more than 50% of the wall, the maximum ablated region is < 70 μm for stainless steel and < 30 μm for graphite. Since it is expected that the plasma energy will be deposited over a major fraction (> 50%) of the first wall during a disruption, it is concluded that both wall materials should withstand a moderate number of disruptive events.

## References

1. W. M. Stacey, Jr., et al., "EPR-77: A Revised Design for the Tokamak Experimental Power Reactor," Argonne National Laboratory, ANL/FPP-77-1 (1977).

2. W. M. Stacey, Jr., et al., "Tokamak Experimental Power Reactor Conceptual Design," Argonne National Laboratory, ANL/CTR-76-3 (1976).

3. "Experimental Power Reactor Conceptual Design Study," General Atomic Company, GA-A14000, (1976).

4. H. C. Stevens, et al., "Tokamak Experimental Power Reactor Primary Energy Conversion System," Second Topical Meeting Technology of Controlled Nuclear Fusion, Richland, Washington, CONF-760935-P4, (September, 1976).

5. "Chrysler Improved Numerical Differencing Analyzer for Third Generation Computers," TN-AP-67-287, Chrysler Corporation (1967).

6. W. M. Stacey, Jr., et al., "Plasma Engineering Studies for the Tokamak Experimental Power Reactor," Seventh IEEE Symposium on Engineering Problems of Fusion Research, Knoxville, Tennessee (October, 1977).

7. A. A. Abdou, "Nuclear Design of the Blanket/Shield System for a Tokamak Experimental Power Reactor," Nucl. Technol. 29, 7 (1976).

8. S. J. Hakim, and R. J. Henninger, "USEFUL: A Hydrodynamic Code for Treating Flow and Freezing in Annular, Pipe, and Plate Geometries," Argonne National Laboratory, ANL/RAS-77-25, (1977).

9. C. S. Kim, "Thermophysical Properties of Stainless Steel," Argonne National Laboratory, ANL-75-55, (1975).

10. R. T. Dolloff, and J. T. Meers, "Status and Future of Graphite and Refractory Compounds," in High Temperature Materials, II, Interscience Publishers, N.Y., 387 (1963).

11. M. R. Everette, et al., "Dimensional and Physical Property Changes of High-Temperature Reactor Graphites," Carbon 9, 417 (1971).

12. G. B. Engle, "Irradiation Behavior of Nuclear Graphites at Elevated Temperatures," Carbon 9, 539 (1971).

13. M. A. Abdou, and C. W. Maynard, "Calculational Methods for Nuclear Heating — Parts I and II," Nucl. Sci. Eng. 56, 360 (1975).

Table I. Materials Properties for Stainless Steel and Graphite

| Property | Stainless Steel | Graphite |
|---|---|---|
| Density, g/cm$^3$ | 7.9 | 2.0 |
| Thermal Conductivity, w/m·K | 20[a] | 4,10,40 |
| Specific Heat, cal/g·°K | 0.12[a] | 0.45 |
| Heat of Vaporization, Kcal/mole | 85 | 171[b] |
| Vaporization Temperature, °K | 1700 | 2500 |
| Emissivity | | 0.8 |
| Neutron Heating, w/cm$^3$ | 10[c] | 7[c] |

[a] Average value. See Ref. 9 for temperature dependent value used.

[b] Heat of sublimation for graphite.

[c] Surface heating rate for 1 MW/m$^2$ neutron wall loading

Table II. Thermal Responses of Stainless Steel Wall with No Liner

| Wall Loading, MW/m$^2$ | 1 | 1 | 2 |
|---|---|---|---|
| Cycle Time, s | 80 | 95 | 80 |
| $T_{max}$ (38), °C* | 402 | 398 | 479 |
| $T_{min}$ (38), °C | 321 | 319 | 322 |
| $\Delta T_{max}$ (38-39), °C | 48 | 45 | 87 |
| $\Delta T_{min}$ (38-39), °C | 2 | 1 | 4 |
| $T_{max}$ (42), °C | 428 | 421 | 537 |
| $T_{min}$ (42), °C | 386 | 365 | 454 |
| $\Delta T_{max}$ (42-41), °C | 39 | 37 | 74 |
| $\Delta T_{min}$ (42-41), °C | 23 | 16 | 43 |

* Numbers in parenthesis refer to nodes.

Table III. Thermal Responses of Graphite for Different Burn-Cycle Scenarios

| Wall Loading, , MW/m$^2$ | 1 | 1 | 1 | 1 | 2 |
|---|---|---|---|---|---|
| Cycle Time, s | 80 | 95 | 80 | 80 | 80 |
| K (graphite), W/m·°K | 10 | 10 | 4 | 40 | 10 |
| $T_{max}$ (60), °C* | 1545 | 1478 | 1877 | 1371 | 2123 |
| $T_{min}$ (60), °C | 1334 | 1211 | 1631 | 1202 | 1688 |
| $\Delta T_{max}$ (60-57), °C | 256 | 236 | 594 | 69 | 516 |
| $\Delta T_{min}$ (60-57), °C | 122 | 92 | 406 | 24 | 239 |

* Numbers in parenthesis refer to nodes.

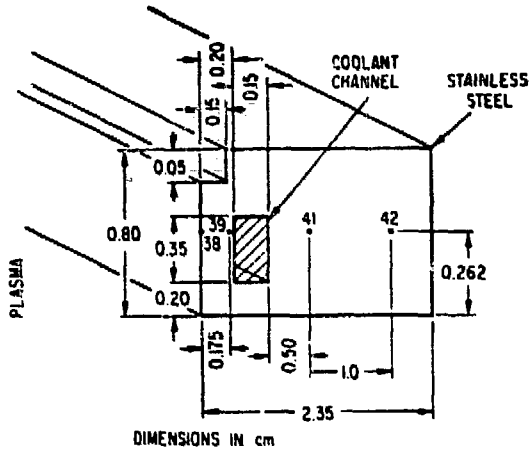


Figure 1. Schematic Diagram of Water-Cooled Stainless Steel First-Wall Design Concept.

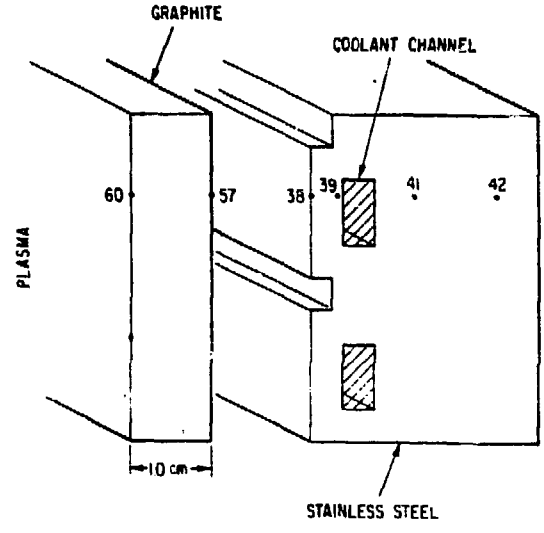


Figure 2. Schematic Diagram of First-Wall Concept With Radiatively-Cooled Graphite Liner

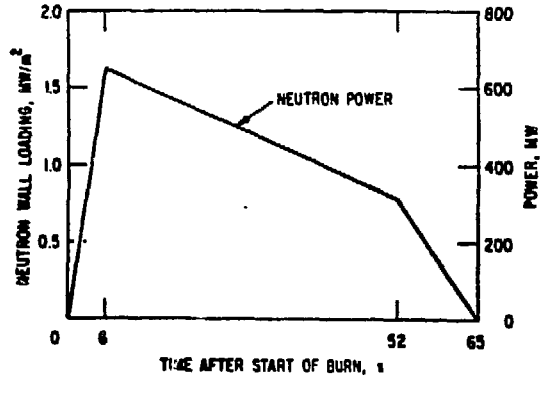


Figure 3. Power Curve for Reference Burn Cycle.

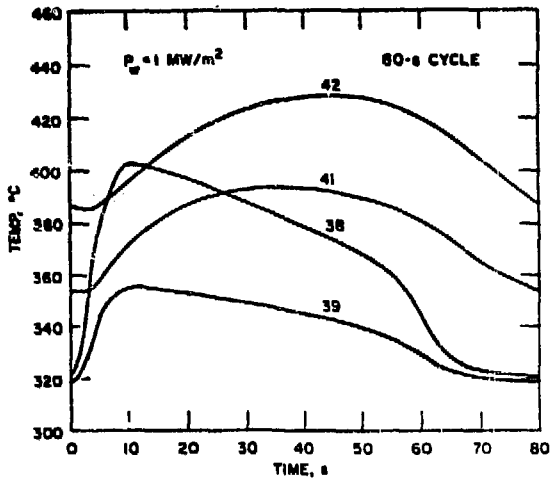


Figure 4. Temperature Response as a Function of Time for Stainless Steel First Wall during Reference Burn Cycle.

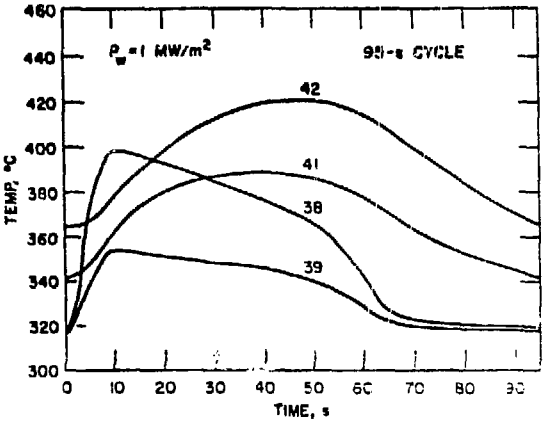


Figure 5. Temperature Response as a Function of Time for Stainless Steel First Wall during Burn Cycle with 30-s Dwell Time.

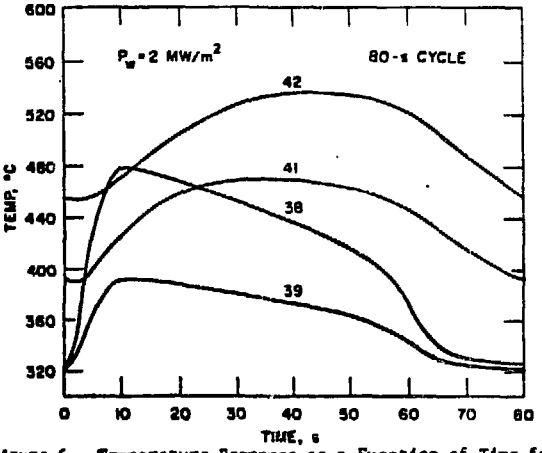


Figure 6. Temperature Response as a Function of Time for Stainless Steel First Wall with 2 MW/m² Average Neutron Wall Loading.

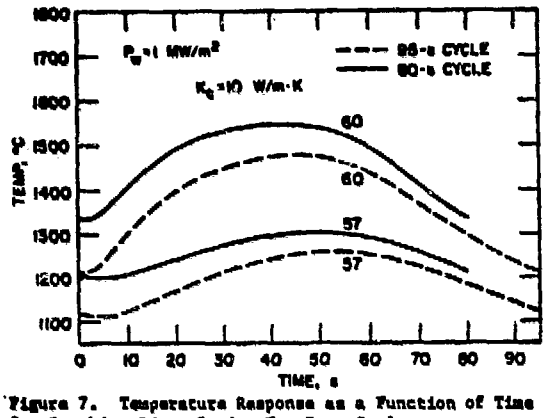


Figure 7. Temperature Response as a Function of Time for Graphite Liner During Two Burn Cycles.

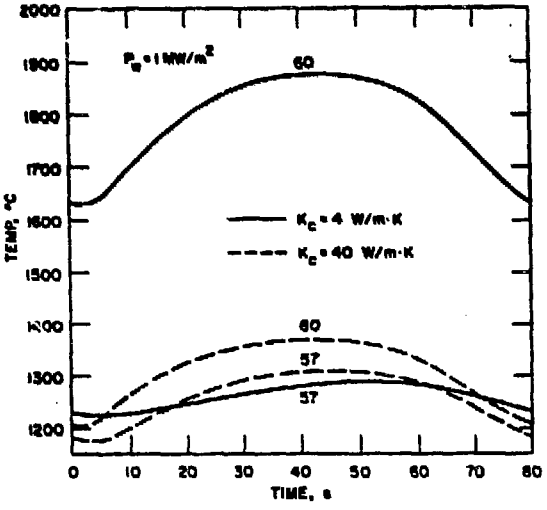


Figure 8. Temperature Response of Graphite Liner Showing Effect of Thermal Conductivity of Graphite.

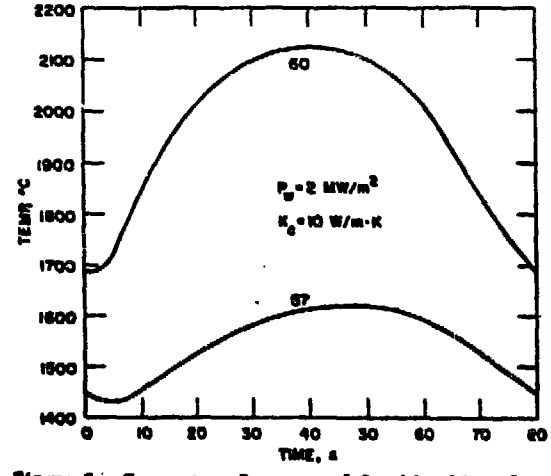


Figure 9. Temperature Response of Graphite Liner for 2 MW/m² Neutron Wall Loading.

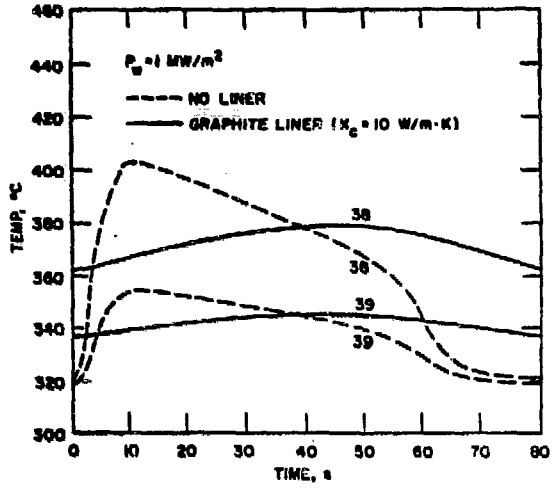


Figure 10. Temperature Response of Stainless Steel Wall With and Without Graphite Liner.

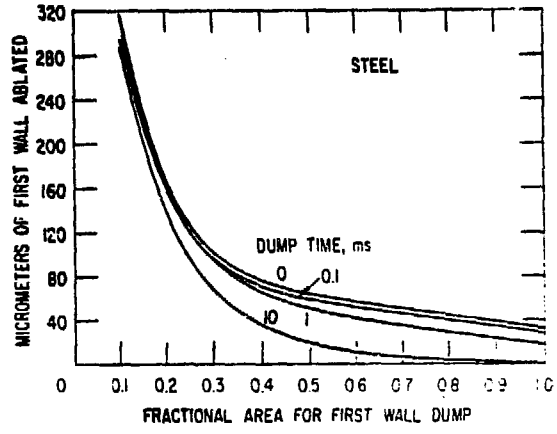


Figure 11. Thickness of Ablated Region of Stainless Steel Wall After Plasma Disruption.

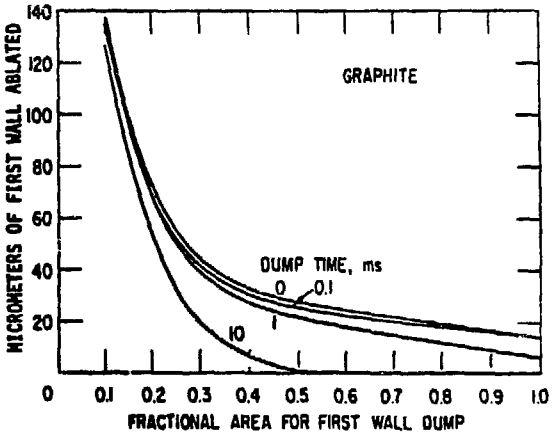


Figure 12. Thickness of Ablated Region of Graphite Wall After Plasma Disruption.